Apparent and Real Absorption of Solar Spectral Irradiance in Heterogeneous Ice Clouds

K. Sebastian Schmidt[1*], Peter Pilewskie[1], Bernhard Mayer[2,3], Manfred Wendisch[4], Bruce Kindel[1], Steven Platnick[5], Michael D. King[1], Gala Wind[5,6], G. Tom Arnold[5,6], Lin Tian[5], Gerald Heymsfield[5], Heike Eichler[7]

[1] University of Colorado, Boulder, CO, USA

[2] Deutsches Zentrum für Luft- und Raumfahrt (DLR), Oberpfaffenhofen, Germany

[3] Ludwig-Maximilians-Universität, München, Germany

[4] Universität Leipzig, Germany

[5] Goddard Space Flight Center, Greenbelt, MD, USA

[6] SSAI, Inc., Lanham, MD, USA

[7] Universität Mainz, Germany

[*] Corresponding author: K. Sebastian Schmidt, Laboratory for Atmospheric and Space Physics, University of Colorado, 392 Campus Box, Boulder, Colorado, USA. Phone: 303-492-6401. Email Sebastian.Schmidt@lasp.colorado.edu

Abstract:

Coordinated flight legs of two aircraft above and below extended cirrus cloud scenes played an important part in the Tropical Composition, Cloud and Climate Coupling (TC^4) Experiment (Costa Rica, 2007). The Solar Spectral Flux Radiometer (SSFR) measured up- and downward irradiance on the high-altitude (ER-2) and the low-altitude (DC-8) aircraft, which allowed deriving apparent absorption on a point-by-point basis along the flight track. Apparent absorption is the vertical divergence of irradiance, calculated by the difference of net flux at the top and bottom of a cloud. While this is the only practical method of deriving absorption from aircraft radiation measurements, it differs from true absorption when horizontal flux divergence is non-zero. Differences between true and apparent absorption are inevitable in any inhomogeneous atmospheres, in particular clouds. We show, for the first time, the spectral shape of measured apparent absorption and compare with results from a three-dimensional radiative transfer model. The model cloud field is created from optical thickness and effective crystal radius retrievals from the MODIS (Moderate Resolution Imaging Spectroradiometer) Airborne Simulator (MAS), and from reflectivity profiles from the Cloud Radar System (CRS), both onboard the ER-2. We find correlations between apparent absorption and cloud optical thickness, especially in the visible spectral range. They bring to bear a net horizontal photon transport from local maxima to minima of optical thickness within a maximum horizontal scale. Although the spectral shape is reproduced by the model calculations, the domain-averaged apparent absorption in the visible spectral range is considerably higher than the model results. This is possibly due to a net loss of photons into neighboring cirrus-free areas that are not contained within the boundaries of the model domain.

1. Introduction

The issue of real versus apparent absorption of solar radiation within clouds was discussed for decades after *Fritz and MacDonald* [1951] discovered cloud absorption derived from measurements may far exceed that from model calculations. Despite its significance for atmospheric energy budget assessments, cloud dynamics, and remote-sensing, a conclusive explanation for this persistent bias is still lacking, and it re-emerges regularly in literature. At best, a status quo was achieved where some authors argued that the problem is ill-posed because the measurement (or model) errors are too large for a final assessment of the bias, while others found model-measurement agreement within the given uncertainties. *Stephens and Tsay* [1990] reviewed the observational evidence for various manifestations of the effect and summarized explanations for the discrepancies. Thereafter, a controversial discussion was initiated by new observations [*Cess et al.*, 1995; *Ramanathan et al.*, 1995; *Pilewskie and Valero*, 1995]. Based on a range of conditions, follow-up studies either rejected [*Hayasaka et al.*, 1995; *Arking*, 1996; *Stephens*, 1996; *Taylor et al.*, 1996; *Francis et al.*, 1997; *Ackerman et al.*, 2003] or supported [*Pilewskie and Valero* 1996, *Valero et al.*, 1997; *Zhang et al.*, 1997; *Valero et al.*, 2000; *O'Hirok et al.*, 2000; *O'Hirok and Gautier*, 2003] the existence of a bias. Many studies favored horizontal photon transport in heterogeneous clouds as cause for the discrepancies [*Newiger and Baehnke*, 1981; *Ackerman and Cox*, 1981; *Rawlins*, 1989; *Titov*, 1998; *Marshak et al.*, 1997, 1998 and 1999] although other explanations were suggested such as enhanced in-cloud water vapor absorption [e.g., *Francis et al.*, 1997; *Arking*, 1999], large drop contributions [*Wiscombe et al.*, 1984; *Ackerman and Stevens*, 1987; *Knyazikhin et al.*, 2002], or in-cloud aerosols [*Newiger and Baehnke*, 1981; *Chylek et al.*, 1984 and 1996, *Wendisch and Keil*, 1999].

Certainly, discrepancies may be caused by a combination of multiple effects, all of which can be ascribed to inappropriate model assumptions or insufficient observations. When attributing shortwave absorption biases to individual causes, adequate spectral resolution in models and measurements to separate the roles of gas and condensed species is highly valuable. For example, absorption by water vapor, aerosol, liquid water or ice can be distinguished by spectral signatures, whether or not the absorption is enhanced due to photon path lengthening in heterogeneous clouds. Most experiments, especially before the late 1990s, did not make use of spectrally resolved measurements. Instruments with full spectral coverage over the solar wavelength range were introduced by *Pilewskie et al.* [2003] and *Wendisch et al.* [2001] for use in aircraft experiments. Despite this important advancement in measurement technology, aspects of the absorption bias problem lingered, for a number of reasons: In typical experiments, absorbed irradiance is derived by differencing net irradiance (difference of downward and upward irradiance) at cloud base and cloud top. This introduces large systematic errors in estimates of cloud absorption because it is the (small) difference of four large quantities. If the measurements above and below clouds are not coordinated in time and space, cloud heterogeneities add further uncertainty. Even if they are coordinated, the measurements may be affected by a net transport of photons through the sides of the sampling volume (net horizontal photon outflux or influx). Horizontal irradiance divergence (convergence) is balanced by the vertical flux divergence which can be misinterpreted as true absorption. We refer to vertical flux divergence as apparent absorption, different from true absorption by the magnitude of horizontal flux divergence.

Horizontal photon transport can be understood in the context of radiative smoothing. Over some scale, contrasts in cloud optical thickness are smoothed out in the corresponding reflectance and transmittance fields [*Marshak et al.*, 1995]. For cloud fields with shadow effects (i.e. clouds with pronounced vertical structure) a roughening can occur as well [*Marshak et al.*, 2006]. For the case of smoothing, the horizontal displacement of a photon relative to its entrance into a cloud field is determined by the number of scatterings which it undergoes. The photon transport is always directed from higher to lower photon density. *Platnick* [2001] shows that this characteristic distance is a function of wavelength (that is, single scattering albedo and asymmetry parameter). In absence of shadows and sources, the horizontal re-distribution of photons in a smoothing process as seen from space (reflectance) can be viewed as transport from optically thick to optically thin regions within the characteristic smoothing scale. The photon path length distribution associated with these processes can be fundamentally different for optically thick regions (diffusion regime) and thin, sparsely populated areas [*Davis and Marshak*, 2000].

Various methods were proposed to correct for horizontal flux divergence in aircraft measurements of absorption. *Ackerman and Cox* [1981] introduced a technique for sampling radiation with a combination of broadband and filter radiometers. Absorption measurements were corrected under the assumption that clouds do not absorb in the visible wavelength range and that radiative smoothing affects non-absorbing and absorbing wavelengths equally. *Marshak et al.* [1999] suggested various correction schemes. One of these explicitly takes into account a pre-determined radiative smoothing scale. Although this improves the Ackerman and Cox method considerably, it does not entirely reproduce the true absorption. *Titov* [1998] (among others) suggested grand-averaging of cloud absorption measurements and provided minimum domain sizes based on typical boundary layer clouds.

In this paper, we pursue a different strategy. Since true absorption is difficult to derive from measurements, we focus on apparent absorption, as obtained from two-aircraft observations, and we reproduce measured apparent spectral absorption (vertical flux divergence) on a pixel-by-pixel basis with 3D radiative transfer (RT) calculations. This strategy is akin to that used by *O'Hirok and Gautier* [2003] who employed ground-based cloud observations as input to 3D RT calculations. We used airborne measurements from the NASA TC^4 experiment (Tropical Composition Cloud and Climate Coupling, Costa Rica, 2007: *Toon et al.*, 2009). An extensive set of instruments was deployed onboard two aircraft, the NASA ER-2 and DC-8. The Solar Spectral Flux Radiometer (SSFR: *Pilewskie et al.*, 2003) was flown on both platforms and measured spectrally-resolved upward and downward solar irradiance. The ER-2 carried the MODIS (Moderate Resolution Imaging Spectroradiometer) airborne simulator (MAS: *King et al.*, 2004), the cloud radar system (CRS: *Li et al.*, 2004), and other remote-sensing instruments. It was operated at 20 km altitude – well above cloud top level. The DC-8 was flown within and below cloud layers and was equipped with instrumentation for cloud microphysical, aerosol particle, and gas-phase measurements. On seven days, the ER-2 and DC-8 were closely coordinated (in space and time) along several flight legs (typically about a 1/2 hour duration per leg) that were chosen in outflow regions near tropical cloud convective cells. In this way, detailed cloud structure data were acquired along with simultaneous above- and below-cloud measurements of solar spectral irradiance. Measurements of cloud-reflected radiance were used for the retrieval of cloud thickness and particle size.

We determined point-by-point apparent spectral absorption for one case and compared with model results. The calculated irradiance fields were obtained from 3D RT calculations, using measurements from MAS and CRS to derive the input cloud field. This paper is the third in a series of three radiation-related publications within the TC^4 special issue (I: *Kindel et al.*: "Observations and modeling of cirrus shortwave spectral albedo during the Tropical Composition, Cloud and Climate Coupling Experiment", II: *Eichler et al.*: "Cirrus spatial heterogeneity and ice crystal shape: Effects on remote sensing of cirrus optical thickness and effective crystal radius"). One aspect of part I is the impact of cloud heterogeneities on radiance-irradiance conversion through cloud retrievals. Part II focuses on the combined effect of scattering phase function and three-dimensional cloud structure on remote-sensing products. This paper (part III) is dedicated to the issue of apparent and real absorption. It starts with a brief description of the instruments, measurement strategy, data processing, generation of the 3D cloud, and of the 3D RT model (section 2). Results are presented in section 3. In the conclusions (section 4), possible implications for remote-sensing and atmospheric energy budget are discussed.

2. Instruments, data, and radiative transfer calculations

SSFR

The SSFR [*Pilewskie et al.*, 2003] measured spectral shortwave irradiance on the ER-2 (above clouds), and on the DC-8 below or within clouds. On both platforms, the up- and down-looking optical inlets were fix-mounted on the aircraft fuselage and connected to rack-mounted spectrometers though optical fibers. The spectral range (350-2150 nm) was covered by using two spectrometers per optical inlet: a grating spectrometer with a Silicon CCD array for near-ultraviolet (NUV), visible (VIS) and very-near-infrared (350-1000 nm, 8 nm spectral resolution) and a spectrometer with Indium-Gallium-Arsenide linear array detector for the shortwave infrared (900-2200 nm, 12 nm resolution) wavelength range. Over the entire range, about 90% of the solar irradiance spectrum is captured. The slit-functions and wavelength-response of the spectrometers were measured in the laboratory prior to the field experiment. An absolute radiometric calibration with a NIST-traceable light source (1000 W lamp) was performed in the laboratory before and after the experiment, and the stability of the calibration was monitored with field-calibrators regularly throughout the experiment. The absolute radiometric accuracy was 3-5% (precision 0.1%). The data were corrected for the angular response of the light collectors and for changes in downward irradiance due to aircraft attitude. The attitude correction was necessary because the light collector reference plane (SSFR horizon) deviated from horizontal alignment due to changes in aircraft pitch, roll, and heading; no active stabilization as described by *Wendisch et al.* [2001] was available for this experiment. In some cases, the attitude correction failed because of reflections from nearby clouds that could not be accounted for by the correction algorithm.

<u>Deriving cloud absorption from SSFR measurements</u>

In aircraft measurements, cloud absorption is derived from the difference of net irradiance, $F_{net} = F^{\downarrow} - F^{\uparrow}$, at the top and bottom of a layer: $\Delta F_V = F_{net,\mathrm{top}} - F_{net,\mathrm{bot}}$ where ΔF_V denotes the vertical component of flux divergence (vertical difference of net irradiance). It differs from true absorption ($F_{\mathrm{abs}} = \Delta F = \Delta F_V + \Delta F_H$) when horizontal flux divergence $\Delta F_H \neq 0$. Due to net horizontal photon transport, ΔF_H is non-zero for any inhomogeneous distribution of atmospheric extinction, in particular in heterogeneous clouds. It is only rarely measured directly. In absence of physical absorbers, $F_{\mathrm{abs}}=0$, and ΔF_H is balanced by ΔF_V that is opposite in sign. The magnitude of ΔF_V is a measure for net horizontal photon transport, and is called apparent absorption. For non-conservative scattering, ΔF_V incorporates real absorption (F_{abs}) and net horizontal transport effects: $\Delta F_V = F_{\mathrm{abs}} - \Delta F_H$. For pronounced horizontal heterogeneity, ΔF_H may dominate ΔF_V, which makes it hard to estimate F_{abs}. The reason why we focus on ΔF_V is that no assumptions about cloud heterogeneity are necessary to derive it, in contrast to F_{abs}.

Fractional absorption (or apparent layer absorptance) is obtained from ΔF_V by normalizing with $F^{\downarrow}_{\mathrm{top}}$. While error analysis is virtually impossible when estimating (F_{abs}) from ΔF_V, it is non-trivial to derive realistic error-estimates even for ΔF_V itself. A brute force method would be combining the radiometric uncertainties (3-5%) with linear error propagation: $e(\Delta F_V) \approx |e(F^{\downarrow}_{\mathrm{top}})| + |e(F^{\uparrow}_{\mathrm{top}})| + |e(F^{\downarrow}_{\mathrm{bot}})| + |e(F^{\uparrow}_{\mathrm{bot}})|$ where e denote systematic absolute instrument uncertainties. However, since all spectrometers are calibrated with the same light source, the errors are not independent. A more realistic uncertainty estimate would be the stability of the spectrometer response functions throughout the experiment (better than 1-2% during TC^4). Another major contributor to total uncertainty is horizontal misalignment of the sensors. Even after correcting for aircraft attitude, a residual error remains. It can exceed radiometric uncertainty [*Wendisch et al.*, 2001] and is hard to derive from theoretical considerations as it depends on the specific measurement situation. We therefore used an empirical estimate of 7% for the maximum total error in downward irradiance. This error subsumes contributions from radiometric calibration, attitude correction, and angular response of the light collectors and was determined by comparing downward modeled and measured irradiance above clouds and in cloud-free areas for all wavelengths (excluding gas absorption bands). For the upward irradiance, we used 5% as maximum error estimate. The net-irradiance error was obtained from linear error propagation: $e(F_{top}) \approx |e(F^{\downarrow}_{top})| + |e(F^{\uparrow}_{top})|$ and $e(F_{bot}) \approx |e(F^{\downarrow}_{bot})| + |e(F^{\uparrow}_{bot})|$. The top-of-cloud and bottom-of-cloud errors were combined by Gaussian error propagation: $e(\Delta F_V) \approx (e(F_{top})^2 + e(F_{bot})^2)^{1/2}$.

<u>MAS</u>

The horizontal cloud structure was inferred from the MODIS Airborne Simulator (MAS). It provided fields of cloud top height, optical thickness (τ) and effective crystal radius (r_{eff}) at a resolution between 50 and 100 m (depending on flight altitude and cloud top height). For high clouds, the cloud top height retrieval was based on the CO_2 slicing technique as used by MODIS [*Menzel et al.*, 2008]. The algorithm that normally uses four CO_2 MODIS channels was adapted to use the three channels available on MAS. For low clouds, the algorithm reverts to the IR window method. The retrieval of optical thickness and crystal effective radius was based on *Nakajima and King* [1990]: For each pixel, reflectance pairs in a visible (or very-near-infrared) channel and a near-infrared channel were compared with one-dimensional forward model calculations. While the shorter wavelength channel was chosen outside gas absorption bands and contains mainly information on optical thickness, the longer wavelength near-infrared channel is affected by liquid water or ice absorption and is sensitive to drop or crystal size. The closest match of the observed reflectance with pre-calculated modeled values was used to infer the optical thickness and effective radius pair. For the TC^4 data processing, algorithms similar to the ones used in MODIS collection 5 retrievals were used, where scattering phase function and single scattering albedo for ice clouds rely on calculations by *Baum et al.* [2005]. Liquid water cloud scattering phase functions were calculated from Mie calculations based on gamma drop size distributions with an effective variance of 0.1 [*Platnick et al.*, 2003]. Detailed instrument information and a description of the retrieval algorithm are given in King et al. [2004, 2009]. *Eichler et al.* [2009, this issue] discuss the impact of crystal habit and 3D radiative effects on the retrievals. MAS data collected during TC^4 were compared with MODIS cloud retrievals [*King et al.*, 2009].

<u>CRS</u>

The vertical cloud structure below the ER-2 flight track was derived from the reflectivity profiles measured by the cloud radar system (CRS: *Li et al.* [2004]) onboard the ER-2. The resolution of the reflectivity field are 37.5 meters in the vertical and about 100 meters in the horizontal. The minimum detectable reflectivity is about -28 dBZ for CRS at a distance of 15 km. The reflectivity from CRS has been compared with the reflectivity from another radar at X- band on ER-2 near the cloud top. Near the cloud top, the reflectivities at both radar frequencies are about the same, an indication that the ice particles obey Rayleigh scattering [*Tian et al.*, 2009].

<u>Case from 17th of July, 2007</u>

We selected one of the well-coordinated flight legs from July 17th, 2007 (from 15:20 to 15:35 UTC). Figure 1 shows this flight leg in the larger scale context (Geostationary Operational Environmental Satellite (GOES) infrared image from 15:28 UTC). It was located 300 km south of Panama (around 5°N, 83°W), near the edge of a high-cloud system. The concurrent GOES VIS image (not reproduced here) shows that the cirrus-free area was partly covered by low-level clouds. The Sun azimuth was northeast, at a zenith angle of approximately 35^{o}.

Both aircraft were guided from the mission operation center at the airport in San José using NASA's Real Time Mission Monitor tool (RTMM, http://rtmm.nsstc.nasa.gov/) that allowed the mission manager to coordinate the aircraft within two minutes on the same ground track. Despite the frequent occurrence of coordinated flight legs throughout the experiment, only one case qualified for our study based upon stringent selection criteria: In order to correctly quantify cloud absorption, the bulk of the cloud layer had to be bracketed by the two aircraft. Due to logistical constraints the DC-8 was frequently scheduled to fly only in-cloud; that is, no below-cloud legs were scheduled. Even for the

17^{th} of July case studied here the DC-8 flew almost entirely within the cloud layer. Since no vertical structure was available from MAS, the information from CRS onboard the ER-2 was vital in order to account for the position of the DC-8 within the cloud. Without this information, it would be impossible to match measured and modeled irradiance at the position of the DC-8. A further, less stringent, requirement was that clouds be composed entirely of ice crystals, determined by the pixel-by-pixel thermodynamic phase information from MAS. Finally, only cases where the attitude correction could be applied (pitch and roll angles within certain limits) were used. These three requirements limited the amount of useable data considerably.

Figure 2 shows the MAS-retrieved cloud optical thickness (gridded to 500 m resolution), CRS reflectivity, and the SSFR spectral albedo for the same ER-2 flight leg as in Figure 1. For the upper panel, blue colors correspond to low; red and black colors to high optical thickness. Cloud gaps are represented by white. The length of the scene is 192 km, the width (swath) 17.5 km. In Figure 2, the southeast to northwest flight track is aligned from left to right. The green shaded areas in the CRS panel mark areas where no data were available. The thick black line represents the MAS-derived cloud top height along the ER-2 flight track which captures the cloud top structure rather well. The dotted line indicates the approximate flight altitude of the DC-8, showing that during large portions of the leg, the DC-8 was actually within cloud rather than below. On some sections of the leg, the radar sensed low-level clouds between the surface and 4 km that were decoupled from the high-level outflow of the cell northeast of the flight leg. The bottom panel shows time series of spectral albedo, with the wavelength varying in the vertical. The SSFR albedo is nearly saturated in the visible wavelength range (red values indicating an albedo near unity) in the optically thick cloud regions. The albedo time series (horizontal lines in the albedo panel) exhibits far less variability than the associated cloud optical thickness, mainly due to the hemispherical (geometrical) averaging inherent to irradiance. Some of the wavelengths show minima that correspond to gas absorption bands. Ice absorption bands (for example around 1500 nm can also be distinguished.

<u>Input Cloud Generation</u>

The fields of optical thickness and effective radius from MAS and the reflectance data from CRS were combined to provide the input to three-dimensional radiative transfer calculations. The profile of radar reflectivity Z (in units of dBZ) was used to derive approximate vertical profiles of ice water content ($IWC(z)$, in g m^{-3}) along the flight track following *Liu and Illingworth* [2000]: $IWC = 0.137*Z^{0.64}$. For each vertical profile along the flight track, the column-integrated ice water path (IWP_{CRS}) was calculated. The IWP was also retrieved from MAS: $IWP_{\mathrm{MAS}} = 2/3*\rho_{\mathrm{ice}}*\tau*R_{\mathrm{eff}}$, where ρ_{ice} is the density of ice (approximately 0.925 g cm^{-3}). While the CRS profile was only measured along the center (nadir) track, MAS-derived IWP was available across the entire swath for each point along the track. In the model cloud, the IWC profiles were obtained through $IWC(\mathrm{z}) = IWC_{\mathrm{CRS}}*IWP_{\mathrm{MAS}}/IWP_{\mathrm{CRS}}$. The entire profile was shifted in altitude corresponding to the cloud top height as retrieved by MAS. Due to the lack of other information, the effective radius was set to $R_{\mathrm{eff}}(\mathrm{x,y,z})=R_{\mathrm{eff,MAS}}(\mathrm{x,y})$, which is clearly a simplification because the crystal size distribution in the lower regions of the cloud is fundamentally different from that near the top. The MAS-derived effective radius is representative of the topmost layer of the cloud [*Platnick et al.*, 2000] where ice crystals are often smaller than in lower layers within the cirrus [*Francis et al.*, 1998; *Gayet et al.*, 2004]. However, a considerable part of radiation is absorbed in the uppermost cloud layer. Therefore, the cloud-top effective radius can be regarded as a valid representation for our study.

In summary, all cloud properties (*IWC*, optical thickness, effective radius, and cloud top height) were tied to MAS measurements; the CRS profiles were used to distribute the MAS-derived IWP vertically. Thereby, the CRS profiles (available only below the ER-2 flight track) were used across the entire MAS swath.

The generated 3D cloud was gridded to 500 m horizontal and 1000 m vertical resolution. For testing, a version with 100 m horizontal resolutions was also generated. However, the impact of spatial resolution is not the focus of this particular study, and the high-resolution cloud was not used in the interest of saving CPU time.

Radiative Transfer Calculations

All calculations were done with the libRadtran radiative transfer package by *Mayer and Kylling* [2005]. The generated cloud microphysical properties within the $384 \times 35 \times 20$ boxes ($n_x \times n_y \times$ number of layers) constitutes the main input for 3D RT calculations, along with atmospheric profiles from dropsondes (launched from the DC-8), and from the DC-8 and ER-2 meteorological data (pressure, relative humidity). For the spectral sea surface albedo, data measured by SSFR during CRYSTAL-FACE (Cirrus Regional Study of Tropical Anvils and Cirrus Layers – Florida Area Cirrus Experiment) was used

[*Schmidt et al.*, 2007b]. For the 3D RT calculations, we applied the forward version of the Monte-Carlo code MYSTIC (Monte Carlo code for the physically correct tracing of photons in cloudy atmospheres: *Mayer* [2009]; *Mayer* [1999]) which is embedded in libRadtran (http://www.libradtran.org). The extraterrestrial spectrum by *Kurucz* [1992], averaged over 1 nm bins, was used as top-of-the atmosphere incident solar irradiance spectrum. For the sake of computational efficiency, the scattering phase functions were represented by the Henyey-Greenstein parameterization based on the asymmetry parameter g (the first moment of the phase function). As shown in *Schmidt et al.* [2007b], this approximation is reasonably close to the exact representation of the cloud phase function, at least for sun angles not too far from zenith position. Both asymmetry parameter and single scattering albedo were taken from ray tracing calculations by *Yang and Liou* [1998]. Calculations were performed for nine wavelengths: 400, 450, 500, 600, 700, 800, 850, 1200, and 1600 nm, using 10^9 photons each.

3. Results

As a first step, we compared the measured time series of upward and downward irradiance above (that is, at ER-2 altitude) and below (or within) clouds (that is, at DC-8 altitude) with model results. To this end, the downward irradiance was rescaled such that changes in solar zenith angle (ranging from SZA = 34°-36° during the leg) were compensated using $F^{\downarrow}(SZA_0) = F^{\downarrow}(SZA) \times (\cos(SZA_0)/\cos(SZA))$, where SZA_0 = 35° was used in the model calculations as well. This correction is discussed in *Schmidt et al.* [2007a]. For the ER-2, both upward and downward irradiance agreed within the expected uncertainties for all nine wavelengths. Less agreement was achieved for the DC-8, which was expected because firstly, the CRS profiles were only available directly underneath the ER-2 and do not represent the vertical cloud structure across the entire MAS swath. Secondly, any mismatches in model and measurement altitude translate directly into discrepancies in irradiance values, due to the large vertical gradients of downward and upward irradiance within cloud layers. The net irradiance is less sensitive; for wavelengths outside gas and cloud absorption bands it is expected to be constant with altitude.

The vertical difference of net irradiances on top and at the bottom of the cloud layer, that is, vertical flux divergence (ΔF_V), is shown in Figure 3 for 500 nm. At this wavelength, the clouds themselves do not absorb and atmospheric gas absorption is near zero. No absorbing aerosol particles were present. Therefore, negligible values are expected for F_{abs}. In absence of true absorption, positive values of ΔF_V (apparent absorption) indicate that photons are lost through the sides of the cloud column (ΔF_H<0); negative values (apparent emission) correspond to a net photon gain. The observations (black dots) are shown with error bars that were estimated from the individual absolute uncertainties as explained above. Throughout almost the entire leg, significant apparent absorption is observed that is not balanced by negative values. On average, 0.17 W m^{-2} nm^{-1} are found. In the modeled vertical flux divergence, in contrast, negative and positive ΔF_V values are balanced and $\langle \Delta F_V \rangle$=0 because F_{abs}=0 and $\langle \Delta F_H \rangle$=0. The domain-averaged horizontal photon transport vanishes due to periodic boundary conditions. The bias between observations and model varies between 0 and 0.2 W m^{-2} nm^{-1}. In most areas, the modeled values are within the uncertainty of the observations. In some places, the discrepancies are larger than the error bars, for example at UTC=15.36 h and UTC=15.47 h.

The red line in Figure 3 shows the MAS optical thickness retrievals averaged within the SSFR footprint. The SSFR footprint is defined as a circle from within which 50% of the ER-2-measured upward irradiance originates. Usually, the SSFR footprint diameter is contained within the MAS swath width. As can be seen in Figure 3, local maxima of optical thickness are connected with high values of ΔF_V and thus a net horizontal outflow of photons; local optical thickness minima are related to minima of ΔF_V.

A possible explanation for the discrepancy between observations and model results could be the limited model domain size (given by the MAS swath width). While in the calculations, photons are confined within the model boundaries, they are not restricted in this way in the real world. If the measurement area is surrounded by regions of lower optical depth or even clear sky, a net transport of photons into these regions can occur, in the same way as between areas of different optical thickness *within* the domain. However, there are theoretical limits for the horizontal displacement of photons. For example, the mean horizontal distance traveled by transmitted photons is in the range of cloud geometrical depth [*Marshak et al.*, 1995] (less for reflected photons). Although the GOES IR image shows that there are indeed areas without high clouds southwest of the flight track, they may be too far off to explain the observations.

In addition to the localized radiative smoothing, irradiance fields incur hemispherical (cosine-weighted) averaging of the underlying radiance fields, which could also contribute to the discrepancy. After all, only about 50% of the irradiance originates from within the MAS swath, and the model results can be biased if the clouds outside the domain are not properly represented by the model cloud. Both effects – photon loss into neighboring areas and geometrical averaging – can only be examined by embedding the MAS-based cloud within the larger context of GOES-derived cloud fields. This is beyond the scope of this study. Until radiative transfer calculations in an extend domain prove the explanations brought forward, one cannot rule out other causes for the discrepancies.

Figure 4 illustrates the relationship between cloud optical thickness and ΔF_V. The observations are shown for 500 nm (black dots) and 1600 nm (red dots), as a function of MAS-retrieved optical thickness (averaged over the SSFR footprint). The propagated error from the measurement uncertainties is shown at maximum optical thickness. The error is larger for 500 nm (only negative error bar is shown) than for 1600 nm because 500 nm is near the maximum of the solar spectrum, and ΔF_V is derived from the difference of large (500 nm) as opposed to small (1600 nm) quantities. In this particular case, the values of ΔF_V are comparable in magnitude for the two wavelengths although the processes involved are fundamentally different: At 1600 nm, true absorption by ice crystals prevails. The modeled dependence of F_{abs} on optical thickness is plotted as red line. Observed (small) excursions from the modeled values can be explained by horizontal photon transport: $\Delta F_V = F_{abs} - \Delta F_H$. At 500 nm, in contrast, the true absorption is expected to be close to zero ($F_{abs} \approx 0$), and $\Delta F_V \approx -\Delta F_H$. As discussed before, almost all the observations exhibit positive ΔF_V, whereas the values from the 3D model calculations (blue dots) do not show such a bias.

There is some indication from the model and observations that net transport of radiation occurs from optically thicker to thinner regions. Obviously no 1:1 relationship can be established, partly because net photon transport takes place between *local* maxima and minima of optical thickness. Net transport of radiation is not induced by optical thickness contrasts if they are separated by scales larger than the mean horizontal photon displacement. For example, radiative smoothing, and thus ΔF_H, at 1600 nm is suppressed in comparison to 500 nm because the absorption has a shortening effect on photon horizontal transport distances.

For small optical thickness (5-10 in Figure 4), positive and negative apparent absorption occurs in the model calculations, uncorrelated with the optical thickness itself. These excursions from zero absorption suggest that in areas with sparse or thin cloud cover, other factors than large-scale horizontal cloud distribution dominate photon transport, for example vertical heterogeneities (multiple layers) and interactions with the surface.

In Figure 5, we show the spectral shape of measurement-derived and simulated cloud absorptance (defined as $\Delta F_V/F^{\downarrow}_{top}\times100\%$) in two different areas of the cloud: at UTC=15.38 h (local maximum of τ – red line) and at UTC=15.44 h (local minimum of τ – blue line), both of which are marked in Figure 3. Results from the 3D model runs are shown as red and blue symbols. The black line shows the absorptance spectrum obtained when averaging observations over the entire leg from UTC=15.33 h – 15.53 h. In the VIS and very-near-infrared, the averaged spectrum is close to the high optical thickness case, the opposite is true the NIR wavelength range. Domain-averaged model results from the independent pixel method are shown as dotted black line.

In all spectra, ice absorption effects are clearly visible in the NIR wavelength range (e.g., around 1500 nm and 2000 nm). Furthermore, the oxygen A-band around 762 nm, and water vapor absorption at 940 nm, 1140 nm and 1350 nm can be distinguished. The water vapor absorption is rather weak because at high altitudes, water vapor concentration is low. In the cases presented here, considerable apparent absorption (up to 20%) is found all across the visible wavelength range, with an upward slope at wavelengths short of 450 nm. For the higher optical thickness case, the spectral behavior is reproduced by the 3D calculations (squares), although not equally across the spectrum (for example, 800 and 850 nm). This gives us some confidence that the observed effects are not measurement artifacts. Above 500 nm, the range of uncertainty of absorptance excludes zero, and the apparent absorption effect is statistically significant. For the low optical thickness case, the 3D model predicts near-zero apparent absorption across most of the visible range. At 1200 nm, the model results fall only marginally within the range of uncertainty of the observations. The domain-averaged independent pixel approximation (IPA) model results do not reproduce the apparent absorption at VIS and very-near-infrared wavelengths. This is expected because horizontal photon transport is ignored by IPA (ΔF_H=0), thus ΔF_V=F_{abs}=0. In the NIR range, IPA over-predicts cloud absorption. A possible reason is that on the domain-average, the MAS-derived effective radius is overestimated [*Eichler et al.*, 2009] which implicates higher NIR absorption. The cross-over between under- and overestimation of absorptance by IPA with respect to the observations is located at about 1400 nm.

The spectral shape in Figure 5 indicates that in high optical thickness areas, the broadband-integrated value of ΔF_V consists of significant contributions from ΔF_H (mainly from below 1400 nm) as well as F_{abs} (from above 1400 nm). In extreme cases, ΔF_H can exceed F_{abs}. In our case, the observed broadband absorption, averaged over the flight leg, amounts to 187 W m-2, contrasted by only 81 W m-2 modeled by IPA that ignores horizontal photon transport.

The reason for the spectral slope at the shortest wavelengths is not entirely understood. It is likely due to a combination of molecular scattering and wavelength-dependent horizontal photon transport. *Marshak et al*. [2008] described a related effect for radiance, the so-called "bluing of the atmosphere" around clouds. Since molecular scattering is stronger at short wavelengths, enhanced reflected radiation near cloud edges gets scattered more effectively at short ("blue") wavelengths and is redirected into satellite sensors. This mechanism could also play a role in explaining the irradiance-based effect that is described here. At very short wavelengths, the apparent absorption becomes negative, leading to an apparent emission of irradiance in the near-UV to blue spectral range.

The spectral signature of the apparent absorption may prove important for cloud and aerosol remote sensing. If the reflectance at different wavelengths responds differently to cloud heterogeneity effects, this has consequences for cloud retrievals. This spectral aspect of cloud retrieval biases occurs in addition to various 3D effects that have been discussed in the literature. Due to the different spatial scales, this additional effect may be more important for cirrus than for boundary layer clouds. A further implication is that any retrieval based on reflectance ratios in the near-UV and visible wavelength range, such as the aerosol index, will be distorted in the presence of cirrus, or other clouds. Regarding the correction technique by *Ackerman and Cox* [1981], the choice of a visible wavelength able to correct for net horizontal photon transport in absorption measurements appears to be problematic, since it is not constant even throughout the non-absorbing part of the spectrum. Related techniques are not as dependent on the spectral signature. However, they often rely on the assumption that horizontal photon transport is comparable for non-absorbing and absorbing wavelengths, which is not the case.

4. Conclusions

In this paper, we studied measured and modeled solar spectral absorption, based on data from the NASA TC^4 experiment in Costa Rica (2007). Most previous studies sought to infer true absorption F_{abs} from measurements of vertical flux divergence. This is problematic in heterogeneous clouds where horizontal fluxes occur. Therefore, we focused on apparent cloud absorption (vertical flux divergence ΔF_V), a quantity that comprises net horizontal photon transport (horizontal flux divergence ΔF_H) as well as true cloud absorption, F_{abs}: $\Delta F_V = F_{abs} - \Delta F_H$. We used SSFR measurements of upward and downward spectral solar irradiance onboard the NASA ER-2 and DC-8 aircraft that were flown in stacked formation above and below the outflow of a tropical convective system on the 17^{th} of July, 2007. NASA's aircraft-ground communication tool (RTMM) allowed a close coordination of the two aircraft in time and space. In this way, the cloud field was sampled over more than 192 km, and a time series of apparent absorption was derived from the differences of above and below-cloud net irradiances. In addition, simultaneous cloud remote-sensing data (MAS-derived horizontal distribution of cloud optical thickness, crystal effective radius, and cloud top height, as well as CRS-derived cloud extinction profiles) were available from the high-flying aircraft. This allowed constructing a 3D model cloud that could be used as input to 3D radiative transfer calculations to validate the measurements on a point-by-point basis along the entire flight leg.

For the first time, we were able to determine the spectral shape of the vertical net flux difference (apparent absorption), and to reproduce it with model calculations. We found considerable positive apparent absorption in the visible wavelength range where clouds do not absorb (F_{abs}=0) that could, at least in part, be explained by net horizontal photon transport. Below 500 nm, the apparent absorption decreases with wavelength and can become negative, thus entailing apparent emission of blue to near-UV radiation by clouds. For absorbing wavelengths, no bias between model results and observations was found. Adjustments of the effective radius like in *O'Hirok and Gautier* [2003] were not required. For non-absorbing wavelengths, measured apparent absorption exceeded 3D model calculations at various points along the leg and averaged over the entire leg. We found correlations between local maxima (minima) of optical thickness on the one hand and high (low) values of vertical flux divergence (ΔF_V), suggesting net horizontal photon transport between those areas. The GOES-IR image indicates that the sampled cloud field was surrounded by areas of lower optical thickness or cirrus-free sky which could give rise to a net loss of photons from the sample area (unaccounted for by the model), thus explaining the enhanced value of apparent absorption in the observations. It was, however, beyond the scope of this study to explore if including the areas around the sample cloud in the model calculations would support this hypothesis and thus fully resolve the reasons for previously observed "absorption bias".

An open question is over which scales photons can effectively be transported within clouds, or away from cloud systems into clear-sky areas. For boundary layer clouds, theoretical limits exist for the maximum horizontal photon displacement [*Platnick*, 2001].

On average, the geometrical distance does not exceed the vertical extent of a cloud layer [*Marshak et al.*, 1995]. When sampling clouds over areas that are larger than this distance, the net horizontal photon flux is expected to be balanced ($\langle \Delta F_{\mathrm{V}} \rangle$=0). Those distances might be larger in high-cloud systems, especially when multiple layers are involved. Moreover, the geometrical averaging inherent to irradiance introduces different effects for boundary layer clouds and large-scale convection systems, just because of the different dimensions. *Kindel et al.* [2009] (Figure 11) shows that irradiance-based retrievals of cloud optical properties of anvils are biased low with respect to radiance-based counterparts, because of the influence of clear-sky areas beyond the imager's swath.

A different manifestation of net horizontal photon transport was observed by *Eichler et al.* [2009], using the same model cloud as employed in this study. The net outflow of photons from optically thick areas makes them appear darker and leads to an underestimation of cloud optical thickness by the imager. The opposite effect in optically thin areas does not fully compensate this bias and leads to a net effect of underestimation of optical thickness. As shown above, this effect is not spectrally neutral. The apparent absorption in optically thick areas is decreasingly effective at wavelengths shorter than 500 nm, which leads to a relative enhancement of shorter-wavelength irradiance. Methods that rely on reflectance ratios at different wavelengths such as the aerosol index will thus be heavily affected in the presence of clouds. A further implication of the spectrally-dependent apparent absorption is that the method by *Ackerman and Cox* [1981] for correcting absorption measurements is compromised: It assumes that horizontal photon transport impacts all wavelengths equally and uses an arbitrary non-absorbing wavelength to correct near-infrared measurements. However, the apparent absorption is not equal across the non-absorbing wavelength range and radiative smoothing is wavelength-dependent. Thus the choice of a visible wavelength for corrections becomes somewhat arbitrary.

Forthcoming research in this area should focus on the following questions:

1. Explain the spectral shape of the near-UV and VIS apparent absorption on a theoretical basis.
2. Determine over which scales horizontal photon transport occurs in high-cloud systems and if embedding the MAS cloud scene in the larger context of GOES can resolve the remaining positive bias between model and observation by attributing it to net photon outflow into clear-sky areas.
3. Connect the spectral signature of heterogeneous clouds in the apparent absorption with remote-sensing applications.

Acknowledgements

The first author was funded under the NASA TC^4 project (NNX07AL12G), as were the deployment of MAS (NNX08AR39G) and CRS onboard the NASA ER-2 aircraft. Warren Gore and Antony Trias (NASA Ames Research Center) integrated and calibrated the SSFR onboard NASA ER-2 and DC-8, and we thank them for their support during the experiment. Steven Platnick and Paul Newman (NASA Goddard) were ER-2 flight scientists on the 17^{th} of July, 2007. The DC-8 dropsondes were launched by Mike Kurylo and Hal Maring (NASA headquarters). The GOES image was provided by courtesy of NASA Larc. The NASA Earth Science Project Office team managed project logistics in Costa Rica and elsewhere. This paper was partly written while the first author worked as a guest scientist at the Meteorological Institute of the University for Natural Resources and Applied Life Sciences in Vienna. Thanks to the colleagues in Austria for their hospitality and discussions.

References

Ackerman, S. A., and G. L. Stephens (1987), The absorption of shortwave solar radiation by cloud droplets: an application of anomalous diffraction theory. *J. Atmos. Sci.*, **44**, 1574-1588

Ackerman, S. A., and S. K. Cox (1981), Aircraft observations of shortwave fractional absorptance of non-homogeneous clouds, *J. Appl. Meteorol.*, **20**, 1510-1515

Ackerman, T. P., D. M. Flynn, and R. T. Marchand (2003), Quantifying the magnitude of anomalous solar absorption, *J. Geophys. Res.*, **109**(D9), 4273

Arking, A. (1999), The influence of clouds and water vapor on atmospheric absorption, *Geophys. Res. Lett.*, **26**, 2729-2732

Arking, A. (1996), Absorption of solar energy in the atmosphere: Discrepancy between model and observations, *Science*, **273**, 779-782

Baum, B. A., A. J. Heymsfield, P. Yang, and S. T. Bedka (2005), Bulk scattering properties for the remote sensing of ice clouds. Part I: Microphysical data and models, *J. Appl. Meteor.*, **44**, 1885–1895

Cess, R. D., M. H. Zhang, P. Minnis, L. Corsetti, E. G. Dutton, B. W. Forgan, D. P. Garber, W. L. Gates, J. J. Hack, E. F. Harrison, X. Jing, J. T. Kiehl, C. N. Long, J.-J. Morcrette, G. L. Potter, V. Ramanathan, B. Subasilar, C. H. Whitlock, D. F. Yound, and Y. Zhou (1995), Absorption of solar radiation by clouds: Observations versus models, *Science*, **267**, 496-499

Chylek, P., G. B. Lesins, G. Videen, J. G. D. Wong, R. G. Pinnick, D. Ngo, and J. D. Klett (1996), Black carbon an absorption of solar radiation by clouds, *J. Geophys. Res.*, **101**, 23365-23371

Chylek, P., V. Ramaswamy, and R. J. Cheng (1984), Effect of graphitic carbon on the albedo of clouds, *J. Atmos. Sci.*, **41**, 3076-3084

Davis, A. B., and A. Marshak (2001), Multiple scattering in clouds: Insights from three-dimensional diffusion/P1 theory, *Nuclear Science and Engineering*, **136**, 251-280

Eichler, H., K. S. Schmidt, R. Buras, M. Wendisch, B. Mayer, P. Pilewskie, M. King, L. Tian, G. Heymsfield, and S. Platnick (2009), Cirrus spatial heterogeneity and ice crystal shape: Effects on remote sensing of cirrus optical thickness and effective crystal radius, submitted to *J. Geophys. Res.*, this special issue.

Francis, P., P. Hignett, A. Macke (1998), The retrieval of cirrus cloud properties from aircraft multi-spectral reflectance measurements during EUCREX '93, *Q.J.R. Meteorol. Soc.,* **124**, 1273-1291

Francis, P. N., J. P. Taylor, P. Hignett, and A. Slingo (1997), On the question of enhanced absorption of solar radiation by clouds, *Q. J. R. Meteorol. Soc.*, **123**, 419-434

Fritz, S., and T. H. MacDonald (1951), Measurements of absorption of solar radiation by clouds, *Bull. Am. Meteorol. Soc.*, **32**, 205-209

Gayet, J. F., J. Ovarlez, V. Shcherbakov, J. Strom, U. Schumann, A. Minikin, F. Auriol, A. Petzold, and M. Monier (2004), Cirrus cloud microphysical and optical properties at southern and northern midlatitudes during the INCA experiment, *J. Geophys. Res.,* **109**, D20206

Hayasaka, T., N. Kikuchi, and M. Tanaka (1995), Absorption of solar radiation by stratocumulus clouds: Aircraft measurements and theoretical calculations, *J. Appl. Meteorol.*, **34**, 1047-1055

Kindel, B. C., K. S. Schmidt, P. Pilewskie, B. Baum, P. Yang, and S. Platnick (2009), Observations and modeling of cirrus shortwave spectral albedo during the Tropical Composition, Cloud and Climate Coupling Experiment, submitted to *J. Geophys. Res.*, this special issue.

King, M. D., S. Platnick, G. Wind, G. T. Arnold (2009), Remote sensing of the radiative and microphysical properties of clouds during TC4: Results from MAS, MASTER, MODIS, and MISR, manuscript in preparation.

King, M. D., S. Platnick, P. Yang, G. T. Arnold, M. A. Gray, J. C. Riedi, S. A. Ackerman, and K. N. Liou (2004), Remote sensing of liquid water and ice cloud optical thickness and effective radius in the Arctic: Application of airborne multispectral MAS data, *J. Atmos. Oceanic Technol.*, **21** (6), 857–875.

Knyazikhin, Y., A. Marshak, W. J. Wiscombe, J. V. Martonchik, and R. B. Myneni (2002), A missing solution to the transport equation and its effect on estimation of cloud absorptive properties, *J. Atmos Sci.*, **59**, 3572-3585

Kurucz, R. L. (1992), Synthetic Infrared Spectra, in Infrared solar physics: proceedings of the 154th Symposium of the International Astronomical Union, edited by D. M. Rabin, J. T. Jefferies, and C. Lindsey, Kluwer Academic Publishers, Dordrecht, the Netherlands, 523-531.

Liu, C., and A. Illingworth (2000), Toward more accurate retrievals of ice water content from radar measurements of clouds, *J. Appl. Meteorol.,* **39**, 1130-1146

Li, L., G. M. Heymsfield, P. E. Racette, L. Tian, and E. Zenker (2004), A 94 GHz cloud radar system on a NASA high-altitude ER-2 aircraft, *J. Atmos. Ocean. Technol.*, **21**, 1378-1388

Marshak, A., G. Wen, J. Coakley, L. Remer, N. G. Loeb, and R. F. Cahalan (2008), A simple model for the cloud adjacency effect and the apparent bluing of aerosols near clouds. *J. Geophys. Res.*, **113**, D14S17, doi:10.1029/2007JD009196.

Marshak, A., S. Platnick, T. Varnai, G. Wen, and R. F. Cahalan (2006), Impact of three-dimensional radiative effects on satellite retrievals of cloud droplet sizes, *J. Geophys. Res.*, **111**(D09207), doi10.1029/2005JD006686

Marshak, A., W. Wiscombe, A. Davis, L. Oreopoulos, R. Cahalan (1999), On the removal of the effect of horizontal fluxes in two-aircraft measurements of cloud absorption, *Q. J. R. Meteorol. Soc.*, **125**, 2153-2170

Marshak, A., A. Davis, W. J. Wiscombe, W. Ridgway, and R. Cahalan (1998), Biases in shortwave column absorption in the presence of fractal clouds, *J. Climate*, **11**, 431-446

Marshak, A., A. Davis, W. Wiscombe, and R. Cahalan (1997), Inhomogeneity effects on cloud shortwave absorption measurement: Two-aircraft simulations, *J. Geophys. Res.*, **102**, 16619-16637

Marshak, A., A. Davis, W. Wiscombe, and R. Cahalan (1995), Radiative smoothing in fractal clouds, *J. Geophys. Res.*, **100**(D12), 26247-26261

Mayer, B. (2009), Radiative transfer in the cloudy atmosphere, *The European Physical Journal Conferences,* **1**, 75-99

Mayer, B., A. Kylling (2005), Technical note: The libRadtran software package for radiative transfer calculations - description and examples of use, *Atmos. Chem. Phys.,* **5**, 1.855-1.877

Mayer, B. (1999), 'I3RC phase 1 results from the MYSTIC Monte Carlo 384 model, paper presented at the I3RC Workshop, NASA, Tucson, Ariz.

Menzel, W. P., R. Frey, H. Zhang, D. Wylie, C. Moeller, R. Holz, B. Maddux, B. A. Baum, K. Strabala, and L. Gumley (2008), MODIS global cloud-top pressure and amount estimation: algorithm description and results. *J. Appl. Meteor. Clim.*, **47**, 1175-1198

Nakajima, T., and M. King (1990), Determination of the optical thickness and effective particle radius of clouds from reflected solar radiation measurements. Part I: Theory, *J. Atmos. Sci.*, **47**, 1878–1893.

Newiger, M., and Baehnke, K. (1981), Influence of cloud composition and cloud geometry on the absorption of solar radiation, *Contrib. Atmos. Phys.*, **54**, 370-382

O'Hirok, W., and C. Gautier (2003), Absorption of shortwave radiation in a cloudy atmosphere: Observed and theoretical estimates during the second Atmospheric Radiation Measurement Enhanced Shortwave Experiment (ARESE), *J. Geophys. Res.*, **108**(D14), doi:10.1029/2002JD002818

O'Hirok, W., C. Gautier, and P. Ricchiazzi (2000), Spectral signature of column solar radiation absorption during the Atmospheric Radiation Measurement Enhanced Shortwave Experiment (ARESE), *J. Geophys. Res.*, **105**(D13), 17471-17480

Pilewskie, P., J. Pommier, R. Bergstrom, W. Gore, S. Howard, M. Rabbette, B. Schmid, P. V. Hobbs, and S. C. Tsay (2003), Solar spectral radiative forcing during the Southern African Regional Science Initiative, *J. Geophys. Res.*, **108**(D13), 8486, doi:10.1029/2002JD002411

Pilewskie, P., and F. P. J. Valero (1996), Response to 'How much solar radiation do clouds absorb?' by G. L. Stephens, *Science*, **271**, 1134-1134

Pilewskie, P., and F. P. J. Valero (1995), Direct observations of excess solar absorption by clouds, *Science*, **267**, 1626-1629.

Platnick, S., M. D. King, S. A. Ackerman, W. P. Menzel, B. A. Baum, J. C. Riedi, and R. A. Frey (2003), The MODIS cloud products: Algorithms and examples from Terra, *IEEE Trans. Geosci. Remote Sens*., **41**, 459–473

Platnick, S. (2001), Approximations for horizontal photon transport in cloud remote sensing problems, *J. Quantitative Spectroscopy and Radiative Transfer*, **68**, 75-99

Platnick, S. (2000), Vertical photon transport in cloud remote sensing problems *J. Geophys. Res.*, 105, 22919-22935

Ramanathan, V., B. Subasilar, G. J. Zhang, W. Conant, R. D. Cess, J. T. Kiehl, H. Grassl, and L. Shi (1995), Warm pool heat budget and shortwave cloud forcing: A missing physics?, *Science*, **267**, 499-503

Rawlins, F. (1989), Aircraft measurements of the solar absorption by broken cloud fields: A case study, *Q. J. R. Meteorol. Soc.*, **115**, 365-382

Schmidt, K. S., V. Venema, F. Di Giuseppe, R. Scheirer, M. Wendisch, and P. Pilewskie: Reproducing cloud microphysical and irradiance measurements using three 3D cloud generators. *Q. J. Royal. Meteorol. Soc.*, **133**, 624, 765-780.

Schmidt, K. S., P. Pilewskie, S. Platnick, G. Wind, P. Yang, and M. Wendisch (2007b), Comparing irradiance fields derived from Moderate Resolution Imaging Spectroradiometer airborne simulator cirrus cloud retrievals with solar spectral flux radiometer measurements, *J. Geophys. Res.*, **112**, D24206, doi:10.1029/2007JD008711.

Stephens, G. L. (1996), How much solar radiation do clouds absorb?, *Science*, **271**, 1131-1133

Stephens, G. L., and S. Tsay (1990), On the cloud absorption anomaly, *Q. J. R. Meteorol. Soc.*, **116**, 671-704

Taylor, J. P., J. M. Edwards, M. D. Glew, P. Hignett, and A. Slingo (1996), Studies with a flexible new radiation code. II: Comparison with aircraft short-wave observations, *Q. J. R. Meteorol. Soc.*, **122**, 839-861

Tian, L., G. M. Heymsfield, A. J. Heymsfield, A. Bansemer, L. Li, C. H. Twohy, and R. C. Srivastava (2009), A study of cirrus ice particle size distribution using TC4 observations, *J. Atmos. Sci.*, in press

Titov, G. A. (1998), Radiative horizontal transport and absorption in stratocumulus clouds, *J. Atmos. Res.*, **55**, 2549-2560

Toon, O. B., D. Starr, E. Jensen, Jucks, M. Kurylo, H. Maring, P. Newman, S. Platnick, M. Schoeberl, P. Wennberg, and Wofsy (2009), The planning and execution of TC4, submitted to *J. Geophys. Res.*, this special issue.

Valero, F. P. J., P. Minnis, S. K. Pope, A. Bucholtz, B. C. Bush, D. R. Doelling, W. L. Smith Jr., and X. Dong (2000), Absorption of solar radiation by the atmosphere as determined using satellite, aircraft, and surface data during the Atmospheric Radiation Measurements Enhanced Shortwave Experiment (ARESE), *J. Geophys. Res.*, **105**, 4743-4758

Valero, F. P. J., R. D. Cess, M. Zhang, S. K. Pope, A. Bucholtz, B. Bush, and J. Vitko, Jr. (1997), Absorption of solar radiation by the cloudy atmosphere: Interpretations of collocated aircraft instruments, J. Geophys. Res., 102, 29917-29927

Wendisch, M., D. Müller, D. Schell, and J. Heintzenberg (2001), An airborne spectral albedometer with active horizontal stabilization, *J. Atmos. Oceanic Technol.*, **18**, 1856-1866

Wendisch, M., and A. Keil (1999), Discrepancies between measured and modeled solar and UV radiation within polluted boundary layer clouds, *J. Geophys. Res.*, **104**, 27373-27385

Wiscombe, W. J., R. M. Welch, and W. D. Hall (1984), The effects of very large drops on cloud absorption, Part I: parcel models, *J. Atmos. Sci.*, **41**, 1336-1355

Yang, P., and K. N. Liou (1998), Single-scattering properties of complex ice crystals in terrestrial atmosphere, *Contributions to Atmospheric Physics*, **71**, 223-248.

Zhang, M., R. D. Cess, and X. Jing (1997), Concerning the interpretation of enhanced cloud shortwave absorption using monthly-mean Earth Radiation Budget Experiment/Global Energy Balance Archive measurement, *J. Geophys. Res.*, **102**, 25899-25905

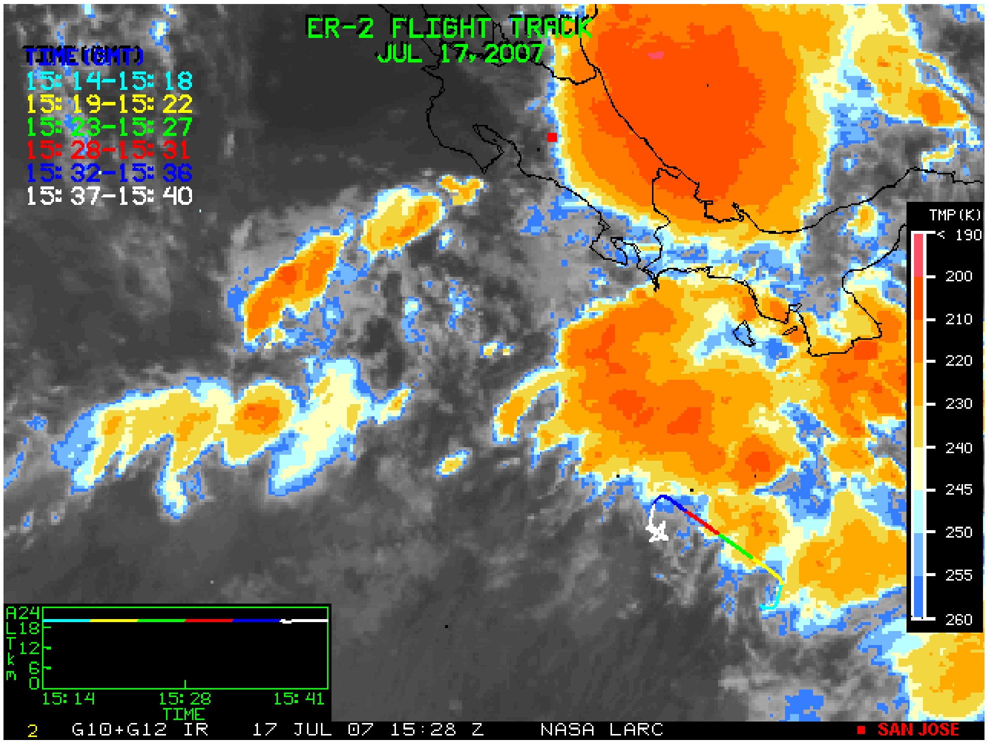

Figure 1 – ER-2 flight leg from 15:20 to 15:35 (straight part of the shown track), in the context of the GOES G10 and G12 IR image from 15:28 UTC. The DC-8 was flown directly underneath. Image courtesy NASA LARC (http://www-angler.larc.nasa.gov/tc4/)

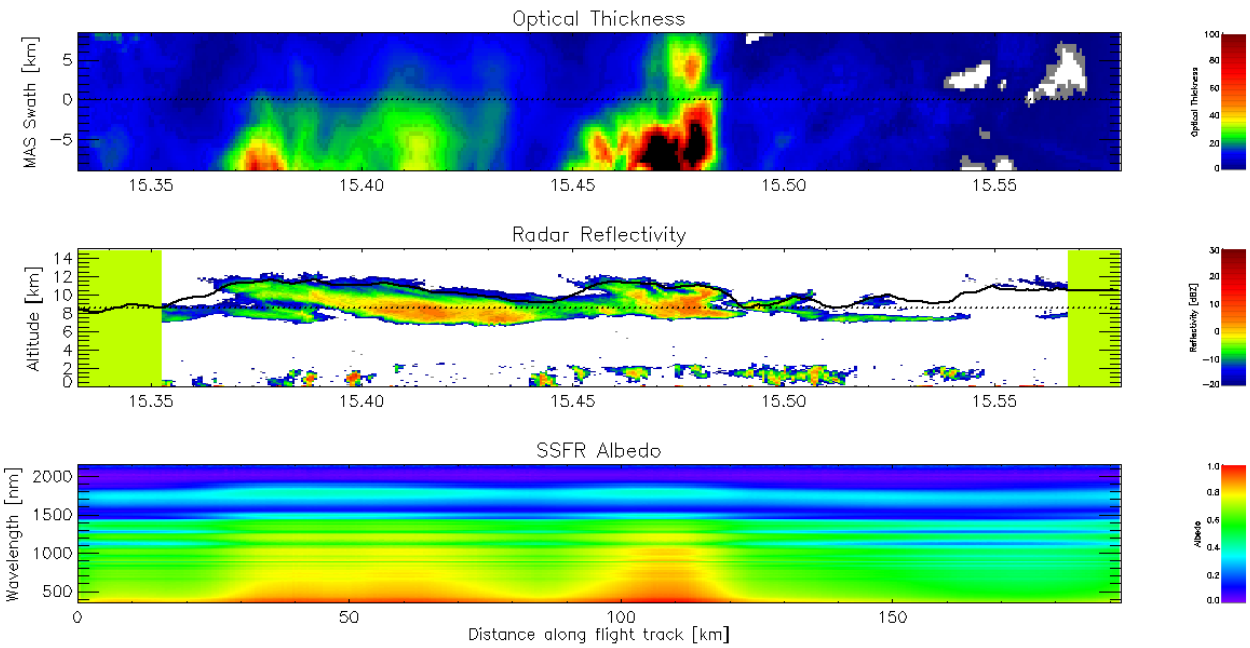

Figure 2 – Data along the 17th of July flight track (15:20 to 15:35 UTC). Top panel: MAS-retrieved cloud optical thickness (swath 17.5 km); below: radar reflectivity from CRS in dBZ. Regions with no data available are marked in light green. Cloud top height from MAS along the ER-2 flight track is over-plotted as thick black line; the dotted line indicates the approximate flight altitude of the DC-8. Bottom panel: ER-2 albedo (wavelength vertical dimension) along the flight track.

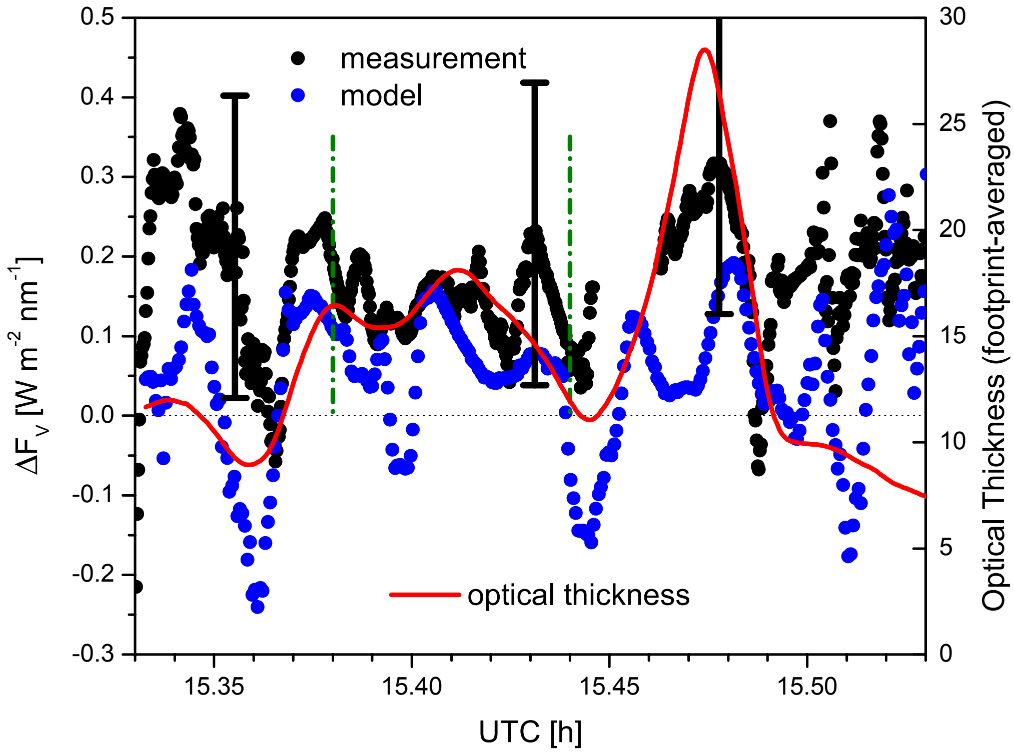

Figure 3 –Time series of measured (black dots) and modeled (blue dots) vertical difference of net irradiances at 500 nm, along with SSFR-footprint-averaged optical thickness (red line). The dash-dotted green lines at UTC=15.35 h and UTC=15.44 h mark where spectra of ΔF_V are shown in Figure 5.

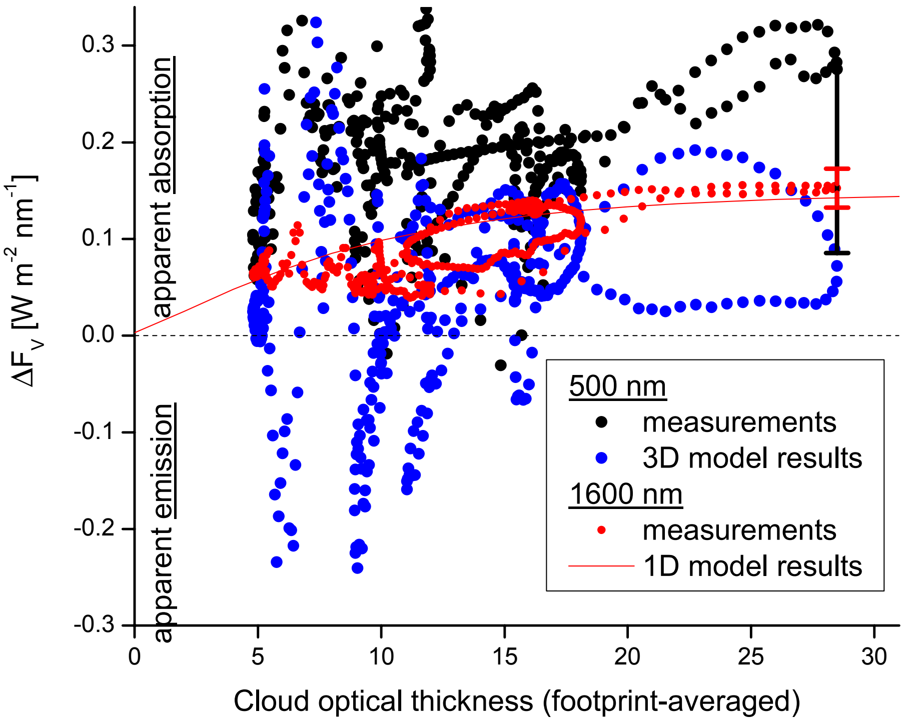

Figure 4 – Measured (black dots) and modeled (blue dots) vertical difference of net irradiances at 500 nm as a function of SSFR-footprint-averaged optical thickness. For comparison, the measurements at 1600 nm are shown (red dots) along with the 1D model true absorption (red line).

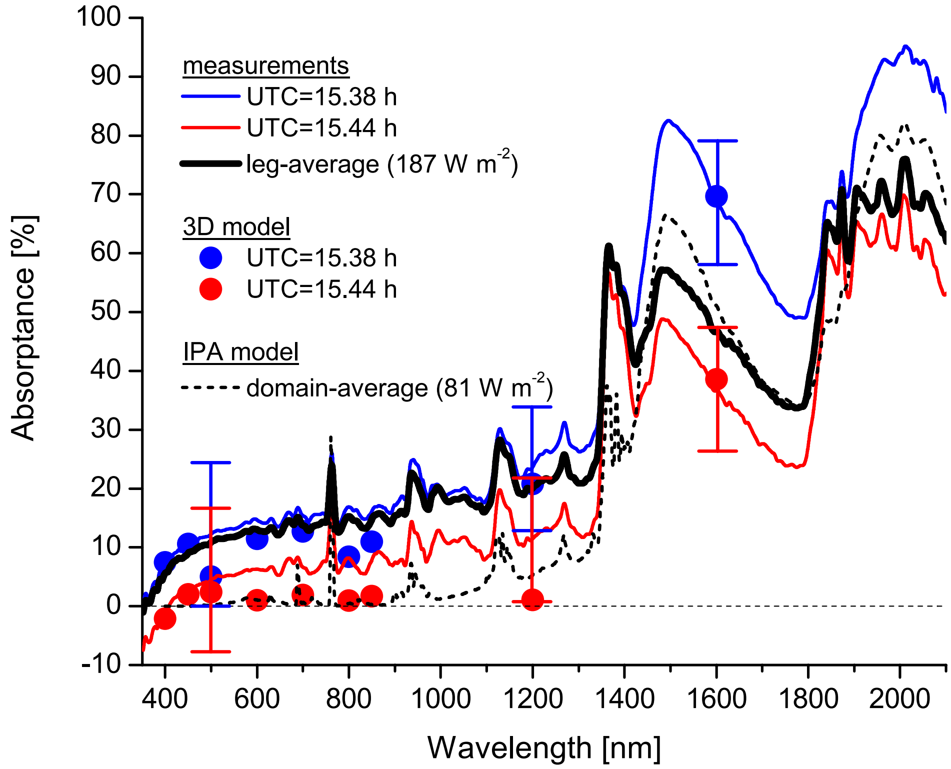

Figure 5 – Spectral absorptance (or fractional absorption) at two selected points along the flight track (UTC=15.44 h – optically thin region, and UTC=15.38 h – optically thick region). The lines show the measurements with ice absorption bands around, for example, 1500 nm. The symbols show model results.